

Monitoring the Transport of Biomass Burning

Emissions in South America

Saulo R. Freitas **

Karla M. Longo

Center for Weather Prediction and Climate Studies - CPTEC/INPE

Maria A. F. Silva Dias

Pedro L. Silva Dias

University of São Paulo

Robert Chatfield - *NASA Ames Research Center*

Elaine Prins – *NOAA/NESDIS/ORA, Madison, WI*

Paulo Artaxo

Fernando S. Recuero

University of São Paulo

Key Words: air pollution, atmospheric modeling, aerosol transport, biomass burning, climate change, long-distance transport, weather forecast

**Corresponding author address: Dr. Saulo R. Freitas

Centro de Previsão de Tempo e Estudos Climáticos – CPTEC/INPE

Rodovia Presidente Dutra, km 39

Cachoeira Paulista, São Paulo, Brazil - ZIP CODE 12630-000

Phone: +55 (12) 3186-8538 - FAX: +55 (12) 3101-2835

Email: sfreitas@cptec.inpe.br

To be submitted to the Environmental Fluid Mechanics

5th RAMS Users Workshop Special Issue

Abstract

The atmospheric transport of biomass burning emissions in the South American and African continents is monitored through a numerical simulation of the air mass motions using the tracer transport capability of the atmospheric model RAMS (Regional Atmospheric Modeling System) coupled to an emission model. In this method, the mass conservation equation is solved for carbon monoxide (CO) and particulate material (PM_{2.5}). Source emissions of trace gases and particles associated with biomass burning activities in tropical forest, savanna and pasture are parameterized and introduced in the model. The sources are distributed spatially and temporally and daily assimilated according to the biomass burning locations detected by remote sensing. The advection, at grid scale, and turbulent transport, at sub-grid scale, are provided by the RAMS parameterizations. A sub-grid transport parameterization, associated with moist deep and shallow convection not explicitly resolved by the model due to its low spatial resolution, is also introduced. Sinks, associated with the process of wet and dry removal of aerosol particles and chemical transformation of gases, are parameterized and introduced in the mass conservation equation. An operational system was implemented producing on a day-to-day basis the 48-hour numerical simulation (24-hour forecast) of the mass concentration for CO and PM_{2.5} in addition to the traditional meteorological fields. Time series of PM_{2.5} measured at the surface level are compared with the model results, and demonstrate the good predictability skill of the model.

1. Introduction

The high concentration of aerosol particles and trace gases observed in the Amazon and Central Brazil atmosphere during the dry season is associated with intense anthropogenic biomass burning activity (vegetation fires). A common estimate is that biomass burning over South America is responsible for the emission of 30 Tg year⁻¹ of aerosol particles to the atmosphere (Andreae, [1]), most of it in the fine fraction of the size distribution which remains in the atmosphere for approximately one week (Kaufman, [2]). Estimates of biomass burning as high as these are disputed by those making detailed studies of subtropical landscapes (Schole et al., [3]), and are thought to vary widely from year to year, (Duncan et al., [3]), and so annual monitoring is an important effort. In addition to aerosol particles, biomass burning produces primarily water vapor and carbon dioxide, emitting also other compounds such as carbon monoxide (CO), volatile organic compounds, nitrogen oxides (NO_x=NO+NO₂), and organic halogen compounds. In the presence of abundant solar radiation and high concentrations of NO_x, the oxidation of CO and hydrocarbons is followed by ozone (O₃) formation.

During the biomass burning season a regional smoke plume covering an area of approximately 4 to 5 million km² has been observed by remote sensing of South America (Prins et al., [4]). Inhalable aerosol particles ($d_p < 10 \mu\text{m}$) with concentration as high as 400 $\mu\text{g m}^{-3}$ have been measured near the surface level and the vertically integrated aerosol optical thickness column reaches 4.0 (440 nm) in Central Brazil. (Artaxo et al., [6][7]; Echalar et al., [8]). The biomass burning particles, made up primarily of organic matter partially oxidized and black-carbon, are highly efficient solar radiation scatters and absorbers; a single scattering albedo of 0.82 has been estimated for these particles (Reid et al., [9]).

On a regional and global scale, the persistent and heavy smoke layer over an extensive tropical region may alter the radiation balance and the hydrological cycling. Modeling efforts of Jacobson [10] and Sato et al. [11] have suggested that the black-carbon radiative forcing could balance the cooling effects of the global anthropogenic sulfate emissions. The direct global radiative forcing of the black-carbon is estimated to be 0.55 Wm^{-2} , corresponding to 1/3 of the CO_2 forcing. This would elevate the black-carbon to one of the most important elements in the global warming, in terms of direct radiative forcing, second only to CO_2 (Andreae, [11]).

The presence of biomass burning particles in the atmosphere may also modify the solar radiative balance by changing the cloud microphysics. These particles act as cloud condensation and ice nuclei, promoting changes in the cloud drops spectrum and, consequently, altering the cloud albedo and precipitation (Cotton and Pielke, [13]; Rosenfeld, [14]). This suggests that biomass burning effects may extrapolate from the local scale and be determinant in the pattern of planetary redistribution of energy from the tropics to medium and high latitudes via convective transport processes.

Several atmospheric pollutants transport models either on regional or global scales have been used. Grell et al., [15] describe a multiscale complex chemistry model coupled to the Penn State/NCAR nonhydrostatic mesoscale model (MM5). Chatfield et al., [16] use the Global-Regional Atmospheric Chemistry Event Simulator (GRACES) to introduce a conceptual model of how fire emissions and chemistry produce the African/Oceanic plumes. Chatfield et al., [17] presents a connection between tropical emissions and an observed subtropical plume of carbon monoxide at remote areas over the Pacific Ocean, using the GRACES and MM5 model. The Georgia Tech/ Goddard Global Ozone Chemistry Aerosol Radiation and Transport (GOCART) is an example of a global transport model. Chin et al., [18] employed GOCART to simulate the

atmospheric global sulfur cycle. MOZART (Model of Ozone And Related Tracers) is another “off-line” global chemical transport model appropriate to simulate the three-dimensional distribution of chemical species in the atmosphere (Brasseur et al., [19]; Horowitz et al., [20]). “Off-line” models mean the transport model is driven using outputs from an atmospheric model previously run or by atmospheric analysis data assimilation. “In-line” transport models have some considerable benefits since they can use the same temporal and spatial resolution of the atmospheric model and, more significantly, they are suitable for feedback studies between the tracers and the atmosphere (as the effects of aerosol on the radiative transfer (Longo et al., 2003 in preparation)).

In this paper a tracer transport model coupled to the Regional Atmospheric Modeling System – RAMS (Walko et al., [21]) is described. The tracer transport simulation is made simultaneously, “in-line”, with the atmospheric state evolution. A real time monitoring transport system is implemented using the coupled transport-atmospheric model. This operational system was designed to forecast and study the transport of biomass burning aerosol and gaseous species in the South American and African continents and applied to the 2002 dry season.

The specification of the biomass burning process related to the source emission parameterization will be described in section 2, the coupled transport-atmospheric model will be presented in section 3 and 4, the results and the dynamical aspects related to the transport of aerosol and gaseous and comparison with observations is seen in section 4. Conclusions and final recommendations are presented in section 5.

2. Main aspects related to the emission and transport of the biomass burning in South America

The ignition, evolution and behavior of a biomass fire and its emissions depend on many factors which are ultimately controlled by the environment. The local climate is relevant in the determination of the amount and characteristics of the biomass available over the ground. For a given type of biomass, the local weather, including temperature, precipitation, humidity and wind, controls the conditions required for the fire ignition and sustenance.

The biomass burning can be described in four basic stages: ignition, flaming, smoldering and extinction (Lobert and Warnatz, [22]). The flaming stage is a pyrolytic process, with the elevated temperatures, as high as 1800 K, breaking apart the biomass molecules and decomposing elements of high molecular weight into elements with lower ones, like coal and tar. Both substances are primary sources of energy for the flames and for the gaseous species released during the flaming combustion, mainly water vapor, CO and CO₂, but also emitting nitrogen oxides, hydrocarbons and an abundance of aerosol particles. The CO and other compounds with uncompleted oxidation and aerosol particles are emitted primarily during the smoldering phase at temperatures typically below 1000 K (Ward et al., [23]). The amount of water in the biomass is one of the most important biomass burning control factors and can determine which stage, flaming or smoldering, will be more significant and define, for example, the ratio between the CO and CO₂ emitted.

Ward et al. [23] estimated the amount of biomass over the ground for Savanna (Campo Limpo, Campo Sujo, Campo Cerrado e Cerrado *Stricto Sensu*) and Primary and Secondary Tropical Forests, ranging from 0.71 to 29.24 kg m² and the combustion factors (percentile of biomass effectively burned) ranging from 52 to 100%, dependent on the vegetation type and the phase of combustion. The higher values for the amount of biomass and lower values for combustion factor were observed for the forest sites.

The emission factor gives the total amount of generic compound emitted in terms of the total biomass consumed. Ward et al. [23] estimate that a Cerrado fire emits on average 1700 g [CO₂]/kg [biomass burned] and 60 g [CO]/kg [biomass burned], while for the forest sites the emission factors were on average 1600 and 125 g/kg for the CO₂ and CO, respectively. For the Cerrado the biomass is primarily consumed during the flaming phase, while for the forest sites this partition was observed to be identical. These results are comparable with the estimates of Ferek et al. [24], based on aircraft measurements conducted during the SCAR-B (Smoke, Clouds and Radiation-Brazil, 1995) field campaign. Average values of CO₂ and CO emission factors of 1700 and 66.5 g/kg were reported for the Cerrado areas, respectively. For forest areas, during the flaming phase, emission factors of 1670 and 70 g/kg were estimated for CO₂ and CO, respectively, contrasting with 1524 and 140 g/kg for the smoldering phase. See Andreae and Merlet [25] for a recent review.

Based on the estimated values of the amount of biomass over the ground (a), the combustion factor (b) and the emission factor (EF), it is possible to estimate the quantity emitted of a certain compound [η] during a burning event if the burning area (a_{fire}) and the type of vegetation can be determined. This can be accomplished using the following equation.

$$M^{[h]} = a_{veg} \times b_{veg} \times EF_{veg}^{[h]} \times a_{fire} \quad (1)$$

The large spatial extent of occurrence of biomass burning over South America makes remote sensing the only feasible way of monitoring these events. Detection of hot spots in the Brazilian Cerrado and Tropical Forest using AVHRR (Advanced Very High Resolution Radiometer), aboard the NOAA polar orbiting satellites series, was developed by Pereira [26] and Setzer and Pereira [27]. Prins and Menzel [28] presented

the monitoring of biomass burning in the Brazilian Cerrado and deforested areas using VAS (Visible Infrared Spin Scan Radiometer Atmospheric Sounder) aboard GOES (Geostationary Operational Environmental Satellite). The technique is based on the difference of the radiative temperatures associated with the two infrared channels (Matson and Dozier [29]). Although the low spatial resolution of the GOES VAS instrument was a limiting factor for monitoring biomass burning, the high temporal resolution was a great advantage, allowing detection of the diurnal variability of fire number and extent. The launch of the GOES-8 Imager in 1994, and the implementation of the ABBA (Automated Biomass Burning Algorithm, version 1.1) for the 1995 biomass burning season represented a significant improvement in the South America fires monitoring (Prins et al., [4]). The resolution of the GOES Imager at nadir (sub-satellite point) is 1 km in the visible and 4 km in the 3.9 and 10.7 micron infrared bands. The instantaneous ground fields of view (IGFOV) are oversampled in the east/west direction by a factor of 1.75 in the visible and IR bands providing a sampled resolution of 0.57 km in the visible band and 2.3 km in the infrared bands at nadir. This oversampling in the east/west can be used to enhance the apparent spatial resolution and allows for increased opportunity to capture an entire fire within one field of view. The ABBA algorithm was developed at CIMSS (Cooperative Institute for Meteorological Satellite Studies) to detect and estimate the size and temperature of biomass fires in South America automatically. Validation tests using prescribed fires in Rondônia State (Northwest of Brazil) reinforced the capability of the ABBA algorithm to identify and estimate instantaneous fire temperature and size for fires on the order of a few acres. Nevertheless, inaccurate corrections for cloud contamination and radiation interaction with the atmosphere can produce overestimates of the fire size. A study of the diurnal variability of the detected number of fires spots for the 1995 burning season showed that

the peak of burning occurs around 17:45 UTC and ranged between 1500 and 3500 spots. The number of fires detected at 17:45 UTC is from 3 to 4 times larger than the number of fires between 14:45 and 20:45 and about 20 times the 11:45 UTC fires detected (Prins et al., [30]). A new version of the GOES-8 ABBA was developed for fire detection and monitoring throughout the western hemisphere. The Wildfire ABBA (WF_ABBA) enables fire monitoring in most ecosystems and was streamlined to allow for rapid processing of half-hourly GOES Imager data for hazards applications and model data assimilation activities. Version 6.0 of the WF_ABBA was implemented during the 2002 fire season in South America.

Biomass burning emits hot gases and particles which are transported upward due to positive buoyancy. The interaction between the smoke and the environment produces eddies that entrain colder environmental air into the smoke plume, which dilutes the plume and reduces buoyancy. The daily turbulent transport in the planetary boundary layer (PBL) produces a well-mixed layer; while horizontal advection transports the plume downwind in the PBL. Dry and wet convective processes and topographic forcing, transport tracers into the middle and upper troposphere. In the troposphere, the pollutants are advected away from the source region. Removal processes are more efficient in the PBL; by the time the pollutants are transported to the troposphere their residence time increases. Several authors (Chatfield and Crutzen, [31]; Pickering et al., [32]; Chatfield and Delany, [33]; Thompson et al., [34]; Chatfield et al., [16]; Freitas et al., [35]; Longo et al., [36]; Freitas et al., [37]; Galanter et al., [38]; Andreae et al., [39]) Chatfield et al., [17]) have been working on the transport of biomass burning emissions in the South American and African continents, mainly focusing on the transport due to wet and deep convective circulations. They have been showing the importance of this mechanism to the vertical distribution of the biomass burning pollutants from the PBL

to the high troposphere with possible implications for regional and global climate change.

3. The atmospheric and the coupled in-line Eulerian tracers transport models

The in-line 3-D model transport follows the Eulerian approach coupled to the RAMS 4.3 parallel version (Walko et al., [21]). RAMS is a numerical model designed to simulate atmospheric circulations at many scales. RAMS solves the fully compressible non-hydrostatic equations described by Tripoli and Cotton [40], and is equipped with a multiple grid nesting scheme which allows the model equations to be solved simultaneously on any number of interacting computational meshes of different spatial resolution. It has a sophisticated set of packages to simulate processes such as: radiative transfer, surface-air water, heat and momentum exchanges, turbulent planetary boundary layer transport and cloud microphysics. The initial conditions can be defined from various observational data sets that can be combined and processed with a mesoscale isentropic data analysis package (Tremback, [41]). For the boundary conditions, it has a 4DDA scheme allowing the atmospheric fields to be nudged towards the large-scale data.

During the dry season, when South America and Africa have a large number of vegetation fires distributed on a continental scale, the computational limitation restrains the model runs to low spatial resolution (on the order of a few tens of kilometers, at least). At this resolution, a cumulus scheme parameterization needs to be introduced because the model is not capable of resolving convection explicitly. New deep and shallow convective schemes based on the mass flux approach (Grell, [42]; Grell and Devenyi, [43]) have been implemented in RAMS 4.3 (Freitas et al 2003, in preparation). The Grell scheme includes moist convective-scale downdrafts and uses as closure the

quasi-equilibrium hypothesis for the determination of the updraft mass flux on the cloud base. This cumulus scheme is suitable for mesoscale runs (horizontal grid spacing about 20 km) and so is adequate for regional transport studies.

The tracer mixing ratio, s ($=\rho/\rho_{\text{air}}$), is calculated using the mass conservation equation

$$\frac{\partial s}{\partial t} = \frac{\partial s}{\partial t} + \frac{\partial s}{\partial t} + \frac{\partial s}{\partial t} + \frac{\partial s}{\partial t} + W_{PM2.5} + R + Q, \quad (2)$$

where the symbols stand for:

- $\frac{\partial s}{\partial t}$, the local tendency,
- adv , the grid-scale advection,
- $PBL\ turb$, the sub-grid turbulent transport in the PBL,
- $deep\ conv$, the sub-grid transport associated with the moist deep convection,
- $shallow\ conv$, the sub-grid transport associated with the moist shallow convection,
- $W_{PM2.5}$, the convective wet removal for PM2.5 (particulate matter with $d_p < 2.5\mu\text{m}$),
- R , the sink term associated with dry deposition and/or chemical transformation,
- Q , the source emission associated with the biomass burning process.

The tracer mixing ratio is updated forward in time using the total tendency given by Eq. (2) and the constant inflow is applied as tracer boundary condition. The next sections will discuss the terms on the right side of Eq. (2).

3.1. The parameterization of the source emission Q

The source emission parameterization is based on the GOES-8 WF_ABBA fire product and field observations. Figure 1 illustrates the technique: inside of each model

grid box there may be observed several sub-grid fires each burning a different type of vegetation. For each fire detected by the GOES-8 WF_ABBA, the mass of the emitted tracer is calculated using Eq. (1) where the type of vegetation burning is given by merging the fire map with the 1 km IGBP 2.0 vegetation map (Belward, [44]), thus allowing the appropriate selection of the vegetation dependent factors of Eq. (1). We shall estimate the burned area by the instantaneous fire size given by the GOES-8 WF_ABBA. For GOES-8 WF_ABBA detected fires that have no information about the instantaneous fire size, the mean instantaneous fire size of 0.14 km² (calculated from the GOES-8 ABBA database of the previous years) is used. The emission in the model follows the diurnal burning cycle described in section 2. The diurnal cycle of the emission is defined by a Gaussian function $r(t)$ centered at 17:45 UTC, normalized to 1 and 8 hours width. In that way, the source emission term is given by

$$Q^{[h]} = \frac{r(t)}{r_0 DV} \dot{a} M^{[h]}_{\substack{\text{fires} \\ \hat{I} \\ \text{Grid_Box}}}, (3)$$

where r_0 is the basic state air density, DV the volume of the first physical grid cell (corresponding to the vertical level $k = 2$) and the mass is calculated over all fires inside the grid cell. The sources are spatially and temporally distributed and daily assimilated by the model according to the biomass burning spots defined by the WF_GOES-8 ABBA. Presently, only the source emissions for CO and PM2.5 have been parameterized.

3.2. The sink term R

The generic process of removal/transformation of tracers (dry deposition for PM2.5 and chemical transformation for CO) is summarized through the term R given by

$$R = - \frac{S}{I}, (4)$$

where the lifetime I is defined as 30 days, for CO (Seinfeld and Pandis, [45]) and 6 days, for PM2.5 (Kaufman, [2]). The PM2.5 tracer quantity represents a monomodal submicron aerosol not significantly affected by coalescence or condensation of further material. This seems to be an adequate description for smoke for the period of a few hours after emission through to the point of significant interaction with cloud and a high probability of removal (Longo et al., in preparation). The major uncertainties in the mass loading and optical effects that we are addressing concern emission strength and wet removal efficiency, and these are large effects in our chosen problem.

3.3. The parameterized deep convective transport and associated wet removal

The deep and moist convection effects on the tracers' distribution are based on the Grell mass flux cumulus scheme. This sub-grid transport tendency is given by,

$$\frac{\partial \langle s \rangle}{\partial t} \Big|_{conv}^{deep} = \frac{m_b}{r_0} \hat{e} \frac{d}{h} \frac{h}{u} (s_u - \tilde{s}) + e \frac{d}{d} \frac{h}{d} (s_d - \tilde{s}) + \tilde{h} \frac{\partial \tilde{s}}{\partial z} \quad (5)$$

Where m_b is the updraft mass flux at cloud base, d is the mass detrainment rate and h is the normalized mass flux, with the subscripts u and d standing for updraft and downdrafts, respectively. e is the ratio between the downdraft and updraft mass fluxes, \tilde{h} is the environment normalized mass flux, s_u , s_d and \tilde{s} stand for tracers mixing ratio in-cloud updraft, downdraft and environment, respectively. The first term on the right side of Eq. 5 corresponds to the updraft mass detrainment, the second to the downdraft mass detrainment and the last to the environment subsidence (advection). For biomass burning tracers usually the PBL is more polluted than the troposphere, so the typical role of the updraft transport is venting the polluted air from the PBL to the high

troposphere where the smoke-laden air is detrained. On the other side, downdraft acts in bringing more pristine air from the mid troposphere into the PBL.

The in-cloud tracer mixing ratio is determined from

$$\frac{ds_{u/d}}{dz} = -m_{u/d} (s_{u/d} - \tilde{s}), \quad (6)$$

$m_{u/d}$ is the up/downdraft entrainment rate and the following boundary condition is used

$$s(z_{u/d}) = \tilde{s}(z_{u/d}), \quad (7)$$

z_u is the updraft cloud base height and z_d is the height level where the downdraft starts.

The coupled convective tracers transport model use the information m_b , $d_{u/d}$, h_{ud} , \tilde{h} , e ,

$m_{u/d}$, z_u and z_d diagnosed from the cumulus scheme in order to determine the value of Eq. 5.

Wet convective removal for PM2.5 is parameterized following Berge [46]. The in-cloud scavenging (washout) is given by

$$W_{PM2.5} = -\frac{Cs_u p}{m_w Dz}, \quad (8)$$

C is the scavenging efficiency, in other words, the probability for aerosols to get embedded in cloud droplets. p and m_w are the precipitation rate and the liquid water content, respectively; and Dz is the thickness of the model layer. The estimated value for C is between 0.53 and 0.71 for smoke (Chuang et al, [47]). The precipitation rate and the liquid water content are both diagnosed by the Grell cumulus scheme and in-cloud tracer concentration is obtained through Eq. 6 after the washout. The sub-cloud precipitation scavenging (rainout) is estimated from

$$W_{PM2.5} = -AMEs_u, \quad (9)$$

M is the concentration of precipitation water (kg [water]/m³), E is the mean collection efficiency averaged over all raindrop sizes and A is a constant term (Berge, [46]).

3.4. The parameterized shallow convective transport

The shallow convective transport follows the same approach described in Eq. 5 disregarding the transport by downdrafts, the wet removal process and it is coupled to the Grell shallow convection scheme (Freitas et al., 2003, in preparation). Here, shallow cumuli act only in venting the aerosol particles and gases from the PBL to the low troposphere.

3.5. The grid scale advection and sub-grid turbulent transport

The grid scale advection and the sub-grid diffusion transport are calculated using the RAMS parameterizations. The horizontal diffusion is based on the Smagorinsky [48] formulation. The vertical diffusion is parameterized according to the Mellor and Yamada [49] scheme, which employs a prognostic of the turbulent kinetic energy. The advection scheme is a forward–upstream of second-order (Tremback et al., [50]).

4. Real time transport monitoring

The operational system follows the scheme depicted in Figure 2. The fires observed by the GOES-8 WF_ABBA on the previous day and the tracers concentration of the last run provide the source emission and the initial condition for the tracers. The CPTEC (Center for Weather Prediction and Climate Studies-Brazil) global analysis and forecast provide the initial and boundary condition for the regional atmospheric model using the 4DDA technique. The model configuration includes 2 grids. The coarse grid has horizontal resolution of 200 km (106 x 41 grid points) covering the South American and African continents. The source emission for the African vegetation fires is prescribed following the Emission Database for Global Atmospheric Research-EDGAR, (Olivier et al, [51]) since the GOES-8 WF_ABBA does not cover this continent. Its

main purpose is to simulate the smoke inflow from the African fires in South America and the long-range transport of smoke from fires on South America to the Atlantic Ocean. The nested grid has a 40 km horizontal resolution (157 x 162) and covers only South America. The vertical resolution for both grids was between 150 to 850 m, with the top of the model at 21 km (33 vertical levels). Each time integration was 48 hours (24 hours forecast). The integration was initiated on 1 July 2002 and carried through successive 48-hour integrations to 30 November 2002. This system has been running on a pc-Linux cluster with 13 processors (Intel-pentium III, 1 GHz) taking about 5 hours of computation.

5. Discussion

From the climatological point of view, central Brazil is dominated from June to September by a high-pressure area with little precipitation and light winds in the lower troposphere (Satyamurti et al., [52]), with convection in the Amazon basin shifted to the northwest part of South America. However, on a day-to-day basis several transient systems may change this picture altering the typical pattern of the smoke transport.

A typical model output represents the tracer (CO or PM_{2.5}) distribution simulated by the biomass burning emissions transport model. Figure 3 (a) shows the CO mixing ratio (ppb) at 1100 m above the surface level at 1800 UTC on 25 August in the regional grid with 40 km resolution. The simulated regional smoke plume had CO concentration values ranging from 100 to 1000 ppb, with maximum values over the places where the fires were mostly distributed. For PM_{2.5}, the simulated values typically ranged from 10 to 500 $\mu\text{g m}^{-3}$ at surface level and 10 to 200 mg m^{-2} for the integrated vertical column. A smoke corridor is evident and it was associated with an anticyclone circulation centered over the Atlantic Ocean. The long-range transport of smoke results in transboundary air pollution with smoke-laden air crossing into South

American countries, like Paraguay, Argentina and Uruguay. Figure 3 (b) shows the CO on a large-scale grid at a resolution of 200 km. A small smoke plume near latitude 45 S and longitude 35 W has traveled about 7000 km. Also seen is the transport of CO from African fires as prescribed by the EDGAR inventory. While there was MOPITT data available (see <http://www.eos.ucar.edu/mopitt/index.html>) for this period, the simulated CO was largely in the boundary layer or hidden by cloud and so largely invisible to that satellite sensor. The MOPITT estimate for 1.5 km suggests around 250 ppb for the portion of South America seen. In Africa, where climatological fire emissions had to be used, the comparison was not quite as good. More consistent comparison between model and MOPITT results is on development.

5.1 A cold front case study

This section describes the typical role of a mid-latitude cold front on the smoke transport and distribution. Figure 4 presents the GOES-8 WF_ABBA fire product depicting over one thousand South American vegetation fires at 1745 UTC on 7 September 2002. Note also the cloudiness associated with a cold front system reaching the polluted boundary layer by the fire emissions. The parameterized CO source emission for this day is shown in Figure 5. The forest biomes in Brazil emitted over 2 ton km⁻² of carbon monoxide. Figure 6 (a) presents the wind field and the temperature (Celsius degrees, contour lines) at 875 m above the surface, at 00 UTC on 27 September 2002, showing the mass convergence line and the enhanced temperature gradient to the south of the convergence line. Shaded contours represent the PM_{2.5} mass concentration vertically integrated (mg m⁻²). An anti-cyclonic flow behind the cold front was outlined after 30 hours of simulation (Figure 6 (b)). The 24 hour (September 7) accumulated rainfall (mm) associated with the cold front as observed by the Tropical Rainfall Measuring Mission (TRMM, Figure 7 a, available at <http://trmm.gsfc.nasa.gov>) and as

simulated by the model (convective (Grell) plus resolved, Figure 7 b). The model simulation has good agreement of the convection location and timing with the TRMM product; nevertheless the model spatial distribution presented more rainfall spread in the North (around 10 N) than shown by TRMM rainfall. The model also simulated less rainfall on the continent, which might be due the difference of the horizontal resolution. The most evident effect of a cold front approaching Central Brazil is the northward transport of the regional smoke plume. Following the cold front approach, the polluted air in central South America is replaced by clean and cold air mass behind it. The smoke is then pushed into the Amazon basin, changing the pristine air pattern, with many climate and chemical implications (Cordoba et al., 2003, in preparation). During these events, it was also observed that the transport of smoke to the Pacific Ocean was enhanced. Less obvious is the effect of the associated convective systems on the particulate and gaseous distribution, as it involves an enhancement of the vertical transport and precipitation and consequent smoke scavenging, including NO_x deposition (via the soluble nitric acid). Figure 8 (a) is a vertical cross section at latitude 13 S showing the high CO concentration in the PBL and the CO vertically transported to the high troposphere by convective systems associated with the cold front. Values over 150 ppb are detrained between a height of 9 and 13.5 km height. Figure 8 (b) shows the plume of CO at the 10700 m (~250 mbar) level being advected by the zonal flow. These simulations agree very well in general pattern and apparently in magnitude with the MOPITT CO estimated for the day. For PM_{2.5}, as it is mainly scavenged by rainfall, the main effect is its deposition over the continent and Atlantic Ocean (Figure 8 (c)), which might have biogeochemical cycling implications. The long-distance transport of poorly soluble gaseous and not scavenged particulate material can be seen in Figure 9. After a cold front event, the high troposphere plume almost crosses the

Atlantic Ocean reaching the Africa continent, typically, one day later. The MOPITT data for the period suggest slightly lower values, but sampling conditions mean that large portions of the plume are not visible.

5.2 Monthly total and means: general export patterns

A South American map, including the model topographic field is provided in Figure 10 as a reference for further discussion. The Andes Mountains, Roraima Mountains and the Amazon basin are depicted, as well as, some Brazilian states (MT for Mato Grosso, RO for Rondonia and PA for Pará), some cities (TA for Tabatinga, SP for Sao Paulo and PtA for Porto Alegre) and, finally, the Jaru forest reserve (JA at Rondonia State).

Figure 11 shows the accumulated carbon monoxide emitted mass (in units of $\text{ton km}^{-2} \text{ month}^{-1}$) for the months of August (a), September (b) and October (c), 2002. It depicts the places in South America where vegetation fires were observed by the GOES-8 WF_ABBA and the amount of CO introduced in the atmosphere prescribed by the biomass burning emission model. In spite of the large number of fires detected in savannas and pastures, in comparison to the number of forest fires, the major amount of the tracers came from forest fires, as the emissions are dependent on the biomass density. Most of these locations are contoured in Figure 11 as $5 \text{ ton km}^{-2} \text{ month}^{-1}$. Some regions like Araguaia Valley (around latitude 9 S and longitude 51W) emitted over $70 \text{ ton km}^{-2} \text{ month}^{-1}$ of CO in August, indicating intense deforestation processes, according to the vegetation map. The Brazilian state Mato Grosso (MT) was the primary source emission over all months, followed by Para (PA) and Rondônia (RO) states. After Brazil, Bolívia was the major significant biomass burning tracer emission country in South America, mostly in October. In addition, in October, an important emission was

noted in North-Northeast Brazil, resulting from deforestation processes in the transition zone between forest and caatinga (the predominant Brazil Northeast biome).

The monthly means of wind field (at 1100 m above the surface) and PM_{2.5} (vertically integrated, mg m⁻²) in the large-scale grid (200 km horizontal resolution) are shown in Figure 12. Most of the mean transport pattern may be explained in terms of the trade winds, the South Atlantic subtropical high pressure system, and the barrier effect of the Andes Mountains. Most of the smoke in the low troposphere was exported to the Atlantic Ocean through the southeast part of South America. In August and September, a small amount of smoke was exported around latitude 8 S to the Pacific Ocean. September showed weaker trade winds producing a more spread out plume compared with August and October patterns. October presented more intense meridional flow, imposing an intense transport of smoke to the south of South America. Still during October, more inflow of smoke into South America from African fires was observed. On a day to day basis, the transport pattern changed due to the occurrence of transient systems like mid-latitude cold fronts or low level jets on the East side of the Andes Mountains.

The monthly meridional and zonal PM_{2.5} mass fluxes (in units of $\mu\text{g m}^{-2} \text{s}^{-1}$) will be now discussed. Figure 13 (a), (c) and (e) show the monthly zonal flux at longitude 40 W and between latitudes 42 S and 10 N. The vertical axis is the height (m) above local surface and the sign convention is positive values for the eastward fluxes. With the exception of September, the maximum zonal fluxes are around 2400 m in elevation. September had the maximum around 4000 m (not shown). These fluxes are mainly related to the occurrence of cold front synoptic systems, when the smoke leaves South America ahead these systems and towards the East. One also can observe that the association of the inflow zonal fluxes to the recirculation and transport from Africa fires

emissions is mostly closer to the surface, and in October the inflow from Africa is much more pronounced as stated before. The meridional fluxes at latitude 35 S are shown in Figure 13 (b), (d) and (f). August revealed a very strong channeled mean flux up to $10 \mu\text{g m}^{-2} \text{ s}^{-1}$ around 55 W and at a height of 2400 m, largely related to the Andes low level jets (Freitas et al., 2003 in preparation) as shown also in Figure 3. The other months had lower meridional fluxes which were more spread out.

Figure 14 shows the same fluxes stated in the last paragraph but at longitude 82 W and the Equator. The transport to the Pacific Ocean took place predominantly around latitude 8 S (Figure 14 a, c and e) and during the month of August. The meridional outward fluxes crossing the Equator (Figure 14 b, d and f) are due to the channeling of the trade winds Northwest of the Amazon Basin by the Andes Mountains to the West and the Roraima Mountains to the East (as shown in Figure 3).

Time series of vertically integrated (mg m^{-2}) PM_{2.5} and CO (ppb) below 3300 m are shown in Figure 15 and Figure 16 for the sites Tabatinga (a), Jaru Reserve (b), São Paulo (c) and Porto Alegre (d) (see Figure 10 for their location). Tabatinga is in the northwest Amazon and is used to monitor the incursion of smoke into the Amazon basin pristine areas. The smoke invasion is well defined by the spikes of the PM_{2.5} column (Figure 15 (a)) and the vertical profiles of CO (Figure 16 (a)). Jaru Reserve is located within a burning region and serves as a local air quality indicator. A very strong boundary layer pollution was pictured during August and September, reaching 250 mg m^{-2} and 2000 ppb for the particulate and CO concentrations, respectively (Figure 15 (b) and Figure 16 (b)). In October, with the onset of the rain season, the smoke was sharply reduced, showing only smoke bursts, time localized, related mainly to the local emissions. São Paulo and Porto Alegre cities (Figure 15, Figure 16; c, d) are included to illustrate the South America smoke outflows and the effects of the regional smoke

plume on the air quality of these cities. The narrow spikes of smoke passing over these cities are evident and were, mostly, associated with the convergence flows due to approaching cold fronts. The smoke plumes typically overpassed the cities almost uncoupled with the surface and may have insignificant effects on the local air quality. A strong outflow overpassing Porto Alegre during October might be seen at Figure 12 (c).

The connection between the narrow spikes at the time series for the Northwest and Southeast sites, which describes the continental exportation of smoke, can be envisioned studying a sequence of events from 25 August to 3 September. Starting on 25 August (Figure 3 (a)), the corridor of smoke was pushed towards the Andes Mountains due to a westward motion of the anti-cyclonic circulation, bringing clean oceanic air to the East and most of Central Brazil. On 28 August, a mid-latitude cold frontal system approached from the Pacific Ocean, pushing the smoke corridor back to the Atlantic Ocean (not shown). At 0600 UTC on 29 August the smoke corridor crossed the low troposphere over Porto Alegre, as is indicated by the narrow spike preceding 1 September in Figure 15 (d). As the cold frontal system moved northward, the smoke corridor at the flow convergence region was pushed to the northeast and, one day later, was crossing São Paulo, as indicated in Figure 15 (c). At the same time, the winds on the Jaru Reserve were from the northwest bringing pristine air from the Amazon basin, which explains the low smoke concentration around 1 September as depicted in Figure 15 (b). As the cold front proceeded, it pushed smoke into the Amazon basin, which was followed by northwest transport by the trade winds. This explains the smoke plume at Tabatinga (Figure 15 (a) and Figure 16 (a)) around 3 September.

Figure 17 presents a comparison between model results and local observation. Time series of PM_{2.5} mass concentration ($\mu\text{g m}^{-3}$) at the first level of the model and from a surface observation at Ji-Paraná site, Rondônia state, are compared. The

measurements represent 30 minutes averages and the model output consists of instantaneous values every 3 hours. The observed data was gathered during the Smoke Aerosols, Clouds, Rainfall and Climate (SMOCC, <http://dionysos.mpch-mainz.mpg.de/smocc>) campaign. The comparison shows very good agreement between the model and observation mainly regarding time variability, although the model values were systematically about 50% below the observation, on average. This comparison suggests that our emission estimates are not overestimates, and possibly underestimates of true emissions. The spatial distribution of the aerosol load (figure not presented) from MODIS derived aerosol product onboard TERRA satellite (http://modis-atmos.gsfc.nasa.gov/MOD04_L2/index.html) is significantly close to the model results, indicating that the model is able to properly represent the transport process.

6. Conclusions

A tracer transport model fully coupled to a regional atmospheric model has been described. An emission model associated with remotely sensed vegetation fires is introduced and a real time operational system was designed to monitor the transport and forecast smoke and gaseous concentrations during the last burning season in the South American and African continents. The pattern and transient transport features are discussed in association with the typical synoptic systems occurring on South America. The model in general presented a good comparison with local observations. The disagreement between the absolute values of PM_{2.5} concentration is due to several factors. The model value represents the grid box average at 40 km horizontal resolution while the observation is local and might not be representative of the model scale. In addition, the GOES-8 Imager resolution limits the detection of smaller fires. Also, the fire area used to estimate the emission actually represents instantaneous measurements of fire size and not the total burned area. Overall, the model was a powerful tool in

understanding the synoptic controls on the biomass burning plume transport and demonstrated good predictability skills.

Acknowledgements

This work was supported by Fundação de Amparo à Pesquisa do Estado de São Paulo (FAPESP), the Millennium Institute "Global and Integrated Advancement of the Mathematics in Brazil" and Projects and Studies Financing Agency (FINEP), Brazil. Part of the model development for this work was done by S. Freitas and R. Chatfield under a grant from US NASA's component of LBA-ECO, RTOP 622-94-13-10.

References

- [1] Andreae, M. O.: 1991, Biomass burning: Its history, use and distribution and its impact on environmental quality and global climate, in *Global Biomass Burning: Atmospheric, Climatic and Biospheric Implications*, ed. by J. S. Levine, pp. 3-21, MIT Press, Cambridge, Mass.
- [2] Kaufman, Y. J.: 1995, Remote Sensing of Direct and Indirect Aerosol Forcing. In: *Aerosol Forcing of Climate*. Ed. by R. J. Charlson and J. Heintzenberg, John Wiley & Sons Ltd.
- [3] Scholes, R. J., D. Ward and C. Justice: 1996, Emissions of trace gases and aerosols particles due to vegetation burning in southern hemisphere Africa. *J. Geophys. Res.*, 101, D19, 23,667-23,676.
- [4] Duncan, B. N., R. Martin, A. Staudt, R. Yevich and J. Logan: 2003, Interannual and seasonal variability of biomass burning emissions constrained by satellite observations. *J. Geophys. Res.*, 108, D2.

- [5] Prins, E. M., J. M. Feltz, W. P. Menzel and D. E. Ward: 1998, An Overview of GOES-8 Diurnal Fire and Smoke Results for SCAR-B and 1995 Fire Season in South America. *J. Geophys. Res.*, 103, D24, 31821-31835.
- [6] Artaxo P., F. Gerab, M.A. Yamasoe and J. V. Martins: 1994, Fine mode aerosol composition in three long-term atmospheric monitoring sampling stations in the Amazon Basin. *J. Geophys. Res.*, 99, 22,857-22,867.
- [7] Artaxo P., E.T Fernandes, J. V. Martins, M.A. Yamasoe, P. Hobbs, W. Maenhaut, K. Longo and A. Castanho: 1998, Large-scale aerosol source apportionment in Amazonia, *J. Geophys. Res.*, 103, 31,837-31,847.
- [8] Echalar, F., P. Artaxo, J. V. Martins, M. Yamasoe, and F. Gerab: 1998, Long-term monitoring of atmospheric aerosols in the Amazon basin: Source identification and apportionment, *J. Geophys. Res.*, 103, 31849-31864.
- [9] Reid, J.S., and P. Hobbs, R. J. Ferek, D. R. Blake, J. V. Martins, M. R. Dunlap, e C. Liousse: 1998, Physical, chemical, and optical properties of regional hazes dominated by smoke in Brazil, *J. Geophys. Res.*, 103, 32,059-32,080.
- [10] Jacobson, M. Z.: 2001, Global direct radiative forcing due to multicomponent anthropogenic and natural aerosols, *J. Geophys. Res.*, 106, D2, 1551-1568, 2001b.
- [11] Sato M., et al.: 2003, Global atmospheric black carbon inferred from AERONET. *Proc. of the Natl. Acad. Sci. USA*, 100, n. 11, 6319-6324.
- [12] Andreae, M. O., The dark side of aerosols, *Nature*, 409, 671-672.
- [13] Cotton, W. R., R. A. Pielke: 1996, Human impacts on weather and climate, Cambridge University Press, New York.
- [14] Rosenfeld D.: 1999, TRMM observed first direct evidence of smoke from forest fires inhibiting rainfall, *Geophys. Res. Lett.*, Vol. 26, N. 20, 3101.

- [15] Grell, G.A., S. Emeis, W. Stockwell, T. Schoenemeyer, R. Forkel, J. Michalakes, R. Knoche and W. Seidl: 2000, Application of a multiscale, coupled MM5/chemistry model to the complex terrain of the VOTALP valley campaign, *Atmos. Env.*, 34, 1435-1453.
- [16] Chatfield, R. B., J. A. Vastano, H. B. Singh and G. Sachse: 1996, A General Model of How Fire Emissions and Chemistry Produce African/Oceanic Plumes (O₃, CO, PAN, smoke). *J. Geophys. Res.*, 101, D19, 24279-24306.
- [17] Chatfield, R. B., Z. Guo, G. Sachse, D. Blake and N. Blake: 2002, The subtropical global plume in the Pacific Exploratory Mission-Tropics A(PEM-Tropics A), PEM-Tropics B, and the Global Atmospheric Sampling Program (GASP): How tropical emissions affect the remote Pacific. *J. Geophys. Res.*, 107.
- [18] Chin, M., R. Rood, S.-J. Lin, J.-F. Muller and A. Thompson: 2000, Atmospheric sulfur cycle simulated in the global model GOCART: Model description and global properties. *J. Geophys. Res.*, 105, 24,671-24,687.
- [19] Brasseur, G.P., D.A. Hauglustaine, S. Walters, P.J. Rasch, J.-F. Müller, C. Granier, and X.X. Tie: 1998, MOZART, a global chemical transport model for ozone and related chemical tracers, 1, Model description, *J. Geophys. Res.*, 103, 28,265-28,289.
- [20] L.W. Horowitz, S. Walters, D.L. Mauzerall, L.K. Emmons, P.J. Rasch, C. Granier, X. Tie, J.-F. Lamarque, M.G. Schultz, G.P. Brasseur, A global simulation of tropospheric ozone and related tracers: Description and evaluation of MOZART, version 2, submitted to *J. Geophys. Res.*, May 2003.)
- [21] Walko R., Band L., Baron J., Kittel F., Lammers R., Lee T., Ojima D., Pélke R., Taylor C., Tague C., Tremback C., Vidale P.: 2000, Coupled Atmosphere-

- Biophysics-Hydrology Models for Environmental Modeling. *J Appl Meteorol* 39:
(6) 931-944.
- [22] Lobert, J. M. and J. Warnatz: 1993, Emissions from the Combustion Process in Vegetation. *Fire in the Environment*, ed. by P. J. Crutzen and J. G. Goldammer. John Wiley & Sons.
- [23] Ward, D. E., R. A. Susott, J. B. Kaufman, R. E. Babbit, D. L. Cummings, B. Dias, B. N. Holben, Y. J. Kaufman, R. A. Rasmussen, A. W. Setzer: 1992, Smoke and Fire Characteristics for Cerrado and Deforestation Burns in Brazil: BASE-B Experiment. *J. Geophys. Res.*, 97, D13, 14601-14619.
- [24] Ferek, R. J., J. S. Reid and P. V. Hobbs: 1996, Emission Factors of Hydrocarbons, Halocarbons, Trace Gases and Particles from Biomass Burning in Brazil. *Smoke/Sulfate, Clouds and Radiation - Brazil (SCAR-B) Proceedings* p. 35-39.
- [25] Andreae, M. O., and P. Merlet.: 2001 Emission of Trace Gases and Aerosols from Biomass Burning. *Global Biogeochemical Cycles*, VOL. 15, NO. 4, 955-966.
- [26] Pereira, M. C. P.: 1988, Detecção, Monitoramento e Análises de alguns Impactos Ambientais de Queimadas na Amazônia usando dados de avião e dos satélites NOAA e LANDSAT. Dissertação de mestrado, INPE-4503-TDL/326, 268 p., Inst.de Pesquisas Espaciais (in portuguese).
- [27] Setzer, A. W., and M. C. Pereira: 1991, Amazonia Biomass Burnings in 1987 and an Estimate of Their Tropospheric Emissions. *Ambio*, 20, 19-22.
- [28] Prins, E. M., and W. P. Menzel: 1992, Geostationary Satellite Detection of Biomass Burning in South America. *Int. J. Remote Sensing*, 13, no. 15, 2783-2799.

- [29] Matson, M. and J. Dozier: 1981, Identification of Sub-resolution High Temperature Sources using a Thermal IR Sensor. *Photogrammetric Engineering and Remote Sensing*, 47, 1311-1318.
- [30] Prins, E. M., W. P. Menzel and D. E. Ward: 1996, GOES-8 ABBA Diurnal Fire Monitoring During SCAR-B. Smoke/Sulfate, Clouds and Radiation – Brazil (SCAR-B) Proceedings. Transtec Editorial, 153-157.
- [31] Chatfield, R. B., and P. J. Crutzen. Sulfur Dioxide in Remote Oceanic Air: Cloud Transport of Reactive Precursors. *J. Geophys. Res.*, 89, D5, 7111-7132, 1984.
- [32] Pickering, K. E., R. R. Dickerson, and G. J. Huffman: 1988, Trace Gas Transport in the Vicinity of Frontal Convective Clouds. *J. Geophys. Res.*, 93759-773.
- [33] Chatfield, R. B., and A. C. Delany: 1990, Convection Links Biomass Burning to Increased Tropical Ozone: However, Models Will Tend to Overpredict O₃. *J. Geophys. Res.*, 95, D12, 18473-18488.
- [34] Thompson, A. M., et al.: 1994, Convective Transport over the Central United States and its Role in Regional CO and Ozone Budgets. *J. Geophys. Res.*, 99, D09, 18703-18711.
- [35] Freitas, S. R., M. A. F. da Silva Dias, P. L. da Silva Dias, K. M. Longo, P. Artaxo, M. O. Andreae and H. Fischer: 2000, A convective kinematic trajectory technique for low-resolution atmospheric models. *Journal of Geophysical Research*, Vol. 105, No. D19, p. 24375-24386.
- [36] Longo, K., A. Thompson, V. Kirchhoff, L. Remer, S. Freitas, M. A. Silva Dias, P. Artaxo, W. Hart, J. Spinhirne, M. Yamasoe: 1999, Correlation between smoke and tropospheric ozone concentration in Cuiabá during Smoke, Clouds, and Radiation-Brazil (SCAR-B). *J. Geophys. Res.*, Vol. 104, No. D10, p. 12113.

- [37] Freitas, S. R., M. A. F. da Silva Dias and P. L. da Silva Dias: 2000: Modeling the convective transport of trace gases by deep and moist convection *Hybrid Methods in Engineering*, vol.2, n. 3, pp. 317-330.
- [38] Galanter, M., H. Levy II, and G. R.: 2000, Carmichael. Impacts of Biomass Burning on Tropospheric CO, NO_x, and O₃, *J. Geophys. Res.*, Vol 105, No. D5, pg. 6633-6653.
- [39] Andreae, M. O., P. Artaxo, H. Fischer, S. R. Freitas, J.-M. Grégoire, A. Hansel, P. Hoor, R. Kormann, R. Krejci, L. Lange, J. Lelieveld, W. Lindinger, K. Longo, W. Peters, M. de Reus, B. Scheeren, M. A. F. Silva Dias, J. Ström, P. F. J. Velthoven and J. Williams: 2001, Transport of biomass burning smoke to the upper troposphere by deep convection in the equatorial region. *Geophys. Res. Lett.*, vol. 28, No. 6, p. 951.
- [40] Tripoli, G. J., e W. R. Cotton: 1982, The Colorado State University Three-Dimensional Cloud/Mesoscale Model. Part I: General Theoretical Framework and Sensitivity Experiments, *J. Rech. Atmos.*, 16, 185-219.
- [41] Tremback, C. J.: 1990, Numerical Simulation of a Mesoscale Convective Complex: Model Development and Numerical Results. Ph.D.Dissertation, Atmos. Sci. Paper No. 465, Colorado State University, Dept. of Atmospheric Science, Fort Collins, CO 80523.
- [42] Grell, G. A.: 1993, Prognostic Evaluation of Assumptions used by Cumulus Parameterization. *Mon. Wea. Rev.*, 121.
- [43] Grell, G. A., and Dezso Devenyi: 2002, A generalized approach to parameterizing convection combining ensemble and data assimilation techniques. *Geophysical Research Letters*, vol. 29, no. 14.

- [44] Belward, 1996 Belward, A.S., ed., 1996, The IGBP-DIS global 1 km land cover data set (DISCover)-proposal and implementation plans: IGBP-DIS Working Paper No.13, Toulouse, France, 61 p.
- [45] Seinfeld, J. H., and S. N. Pandis: 1998, Atmospheric Chemistry and Physics. John Wiley & Sons Ltd., 1326 p.
- [46] Berge, E.: 1993, Coupling of wet scavenging of sulphur to clouds in a numerical weather prediction model. *Tellus*, 45B, 1-22.
- [47] Chuang, C. C., Penner, J. E., and Edwards, L. L. (1992) Nucleation Scavenging of Smoke Particles and simulated Drop Size Distributions over Large Biomass Fires. *J. Atmos. Sci.* No. 14, pp. 1264-1275.
- [48] Smagorinsky, J.: 1963, General circulation experiments with the primitive equations. Part I, The basic experiment. *Mon. Wea. Rev.*, **91**, 99-164.
- [49] Mellor, G.L., and T. Yamada: 1974, A hierarchy of turbulence closure models for planetary boundary layers. *J. Atmos. Sci.*, **31**, 1791-1806.
- [50] Tremback, C.J., J. Powell, W.R. Cotton, and R.A. Pielke: 1987, The forward in time upstream advection scheme: Extension to higher orders. *Mon. Wea. Rev.*, **115**, 540-555.
- [51] Olivier, J.G.J., A.F. Bouwman, C.W.M. van der Maas, J.J.M. Berdowski, C. Veldt, J.P.J. Bloos, A.J.H. Visschedijk, P.Y.J. Zandveld, and J.L. Haverlag: 1996, Description of EDGAR version 2.0: A set of global emission inventories of greenhouse gases and ozone-depleting substances for all anthropogenic and most natural sources on a per country basis and on a 1x1 degree grid, RIVM report 771060 002/TNO-MEP report R96/119, National Institute of Public Health and the Environment, Bilthoven, the Netherlands.

[52] Satyamurty, P., C. A. Nobre, and P. L. Silva Dias: 1998, Meteorology of the Southern Hemisphere. Ed. by D. J. Karoly and D. G. Vincent. AMS, vol. 27, number 49, 119-139.

Captions

Figure 1: Biomass burning source emission parameterization. Fires are sub-grid processes burning different types of vegetation. The total amount of emitted mass is obtained and diluted in the air contained at the model grid box.

Figure 2: General flow of the real time monitoring the transport of biomass burning emissions in South America.

Figure 3: Example of the transport model output. The Figure (a) shows the plume of CO (ppb) at regional model grid (40 km horizontal resolution) on 1800Z August 25, 2002 and 1100 m above surface. Figure (b) depicts the coarse model grid (200 km) covering the South America and part of Africa continents.

Figure 4: The GOES-8 WF_ABBA fire product at 1745 UTC on 7 September 2002 depicting the vegetation fires in the South America. Also shown the cloudiness associated with a cold front synoptic system reaching the polluted boundary layer.

Figure 5: The parameterized CO source emission for September 7, 2002. Some places on Brazil with forest biomes emitted over 2 ton km^{-2} of carbon monoxide.

Figure 6: (a) Wind field and the temperature (Celsius degrees, contour lines) at 875 m above the surface on 00Z September 7. Shaded contour represents the PM2.5 mass concentration vertically integrated (mg m^{-2}). (b) Wind field and PM2.5 mass concentration on 06Z September 8.

Figure 7: (a) September 7 accumulated rainfall (mm) as observed by the Tropical Rainfall Measuring Mission (TRMM), (b) RAMS model simulated (convective (Grell) plus resolved) rainfall for the same period.

Figure 8: (a) Vertical cross section at latitude 13 S of CO (ppb) concentration in the PBL and the CO vertically transported to the high troposphere on 00Z September 8. (b) Plume of CO at level 10700 m (~250 mbar) being advected by the zonal flow. (c) Accumulated PM_{2.5} wet removed (mg m^{-2}) between 00Z 7 – 00Z 8 September.

Figure 9: The long-distance transport of the CO plume at level 10700 m above surface on 00Z September 9 at coarse resolution grid.

Figure 9: Model 40 km resolution topography field of South America.

Figure 11: Accumulate carbon monoxide emitted mass ($\text{ton km}^{-2} \text{ month}^{-1}$) for the months of August (a), September (b) and October (c), 2002 as prescribed by the emission model.

Figure 12: Monthly means of wind field (at 1100 m above the surface) and PM_{2.5} (vertically integrated, mg m^{-2}) at large-scale grid (200 km horizontal resolution) for the months of August (a), September (b) and October (c), 2002.

Figure 13: Monthly meridional and zonal PM_{2.5} mass fluxes ($\mu\text{g m}^{-2} \text{ s}^{-1}$): (a), (c) and (e) show the monthly zonal flux on longitude 40 W and between latitudes 42 S and 10 N

against the height (m) above local surface; (b), (d) and (f) show the meridional fluxes on latitude 35 S. Signal convention is positive values for the outward fluxes.

Figure 14: Monthly meridional and zonal PM2.5 mass fluxes ($\mu\text{g m}^{-2} \text{s}^{-1}$): (a), (c) and (e) show the monthly zonal flux on longitude 82 W and between latitudes 42 S and 10 N against the height (m) above local surface; (b), (d) and (f) show the meridional fluxes on latitude Equator. Signal convention is positive values for the outward fluxes.

Figure 15: Time series of PM2.5 vertically integrated (mg m^{-2}) for the sites Tabatinga (a), Reserve Jaru (b), São Paulo (c) and Porto Alegre (d). Model results between August 1 and October 31, 2002.

Figure 16: Carbon monoxide (CO, ppb) at the first 3300 m above for the sites Tabatinga (a), Reserve Jaru (b), São Paulo (c) and Porto Alegre (d). Model results between August 1 and October 31, 2002.

Figure 17: Time series of PM2.5 mass concentration ($\mu\text{g m}^{-3}$) as simulated by the model (black) and measured at surface (gray) on Ji-Paraná site, Rondônia.

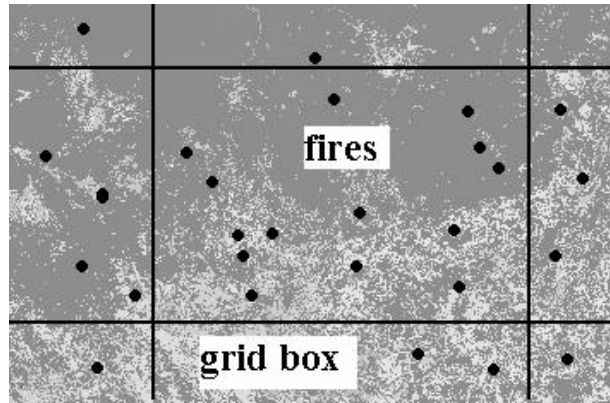


Figure 1

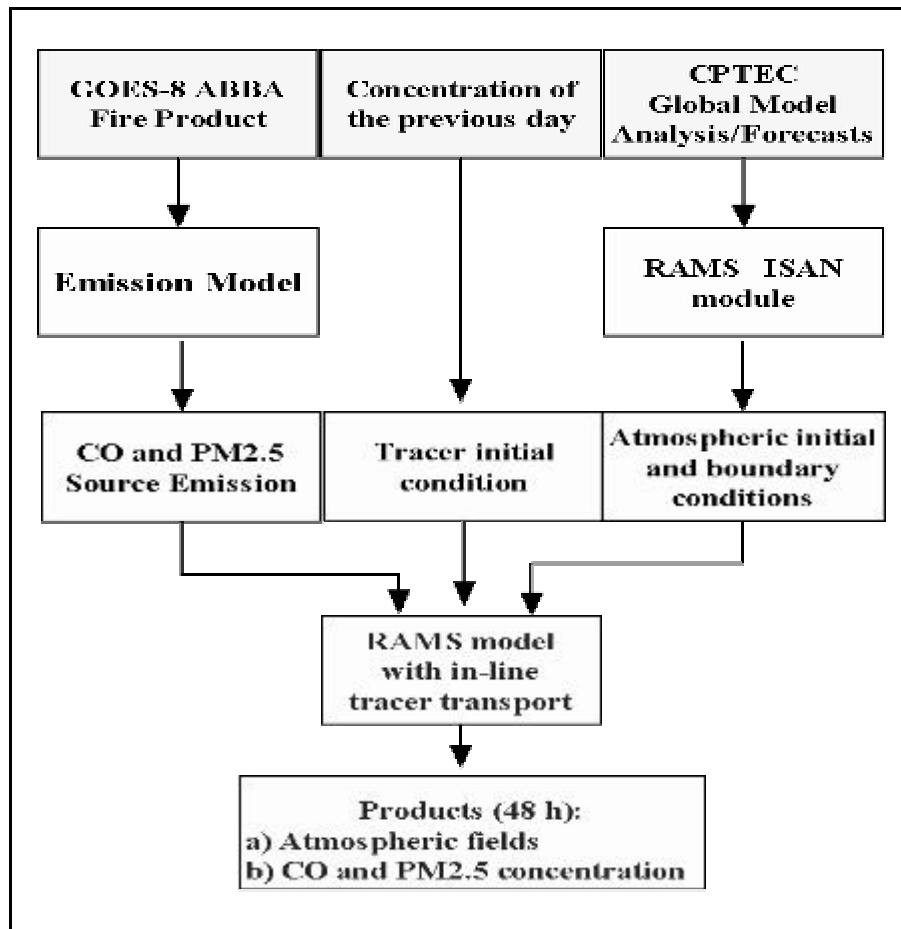
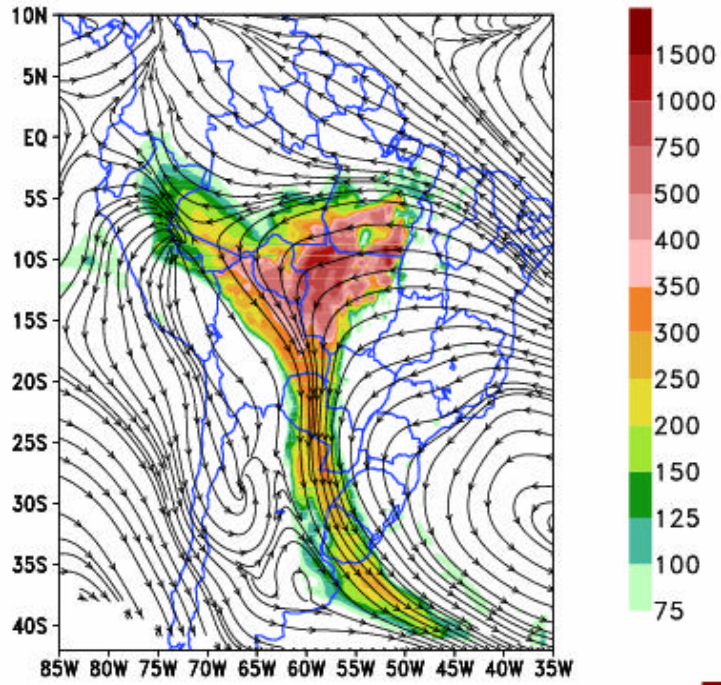


Figure 2

(a) Carbon Monoxide (ppb) - 40km
1100 m - 18Z25AUG2002



(b) Carbon Monoxide (ppb) - 200km

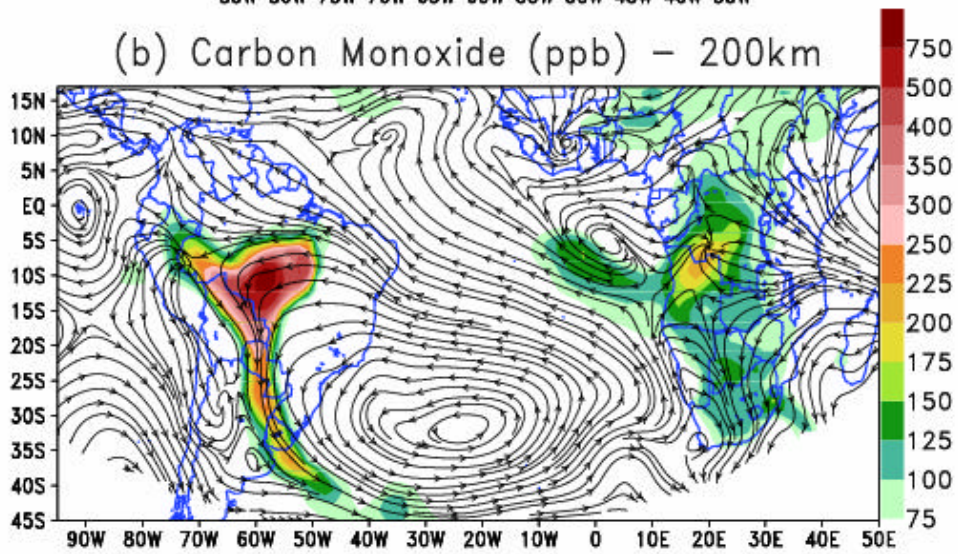


Figure 3

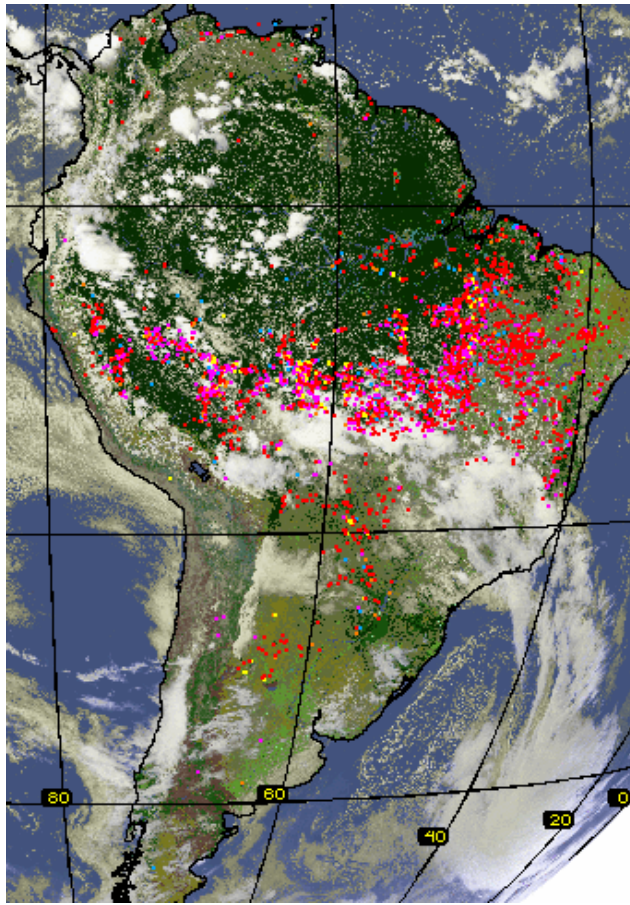


Figure 4

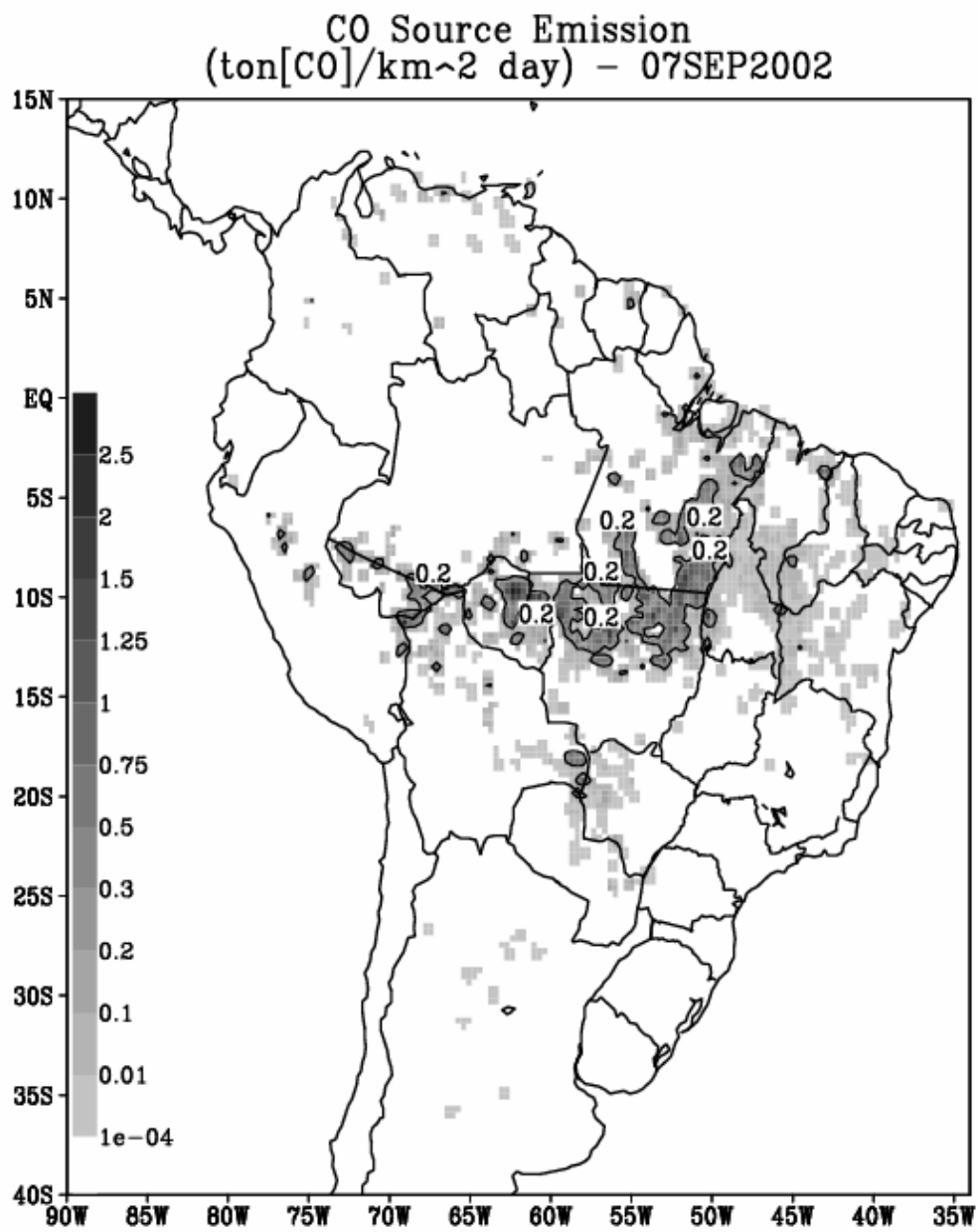


Figure 5

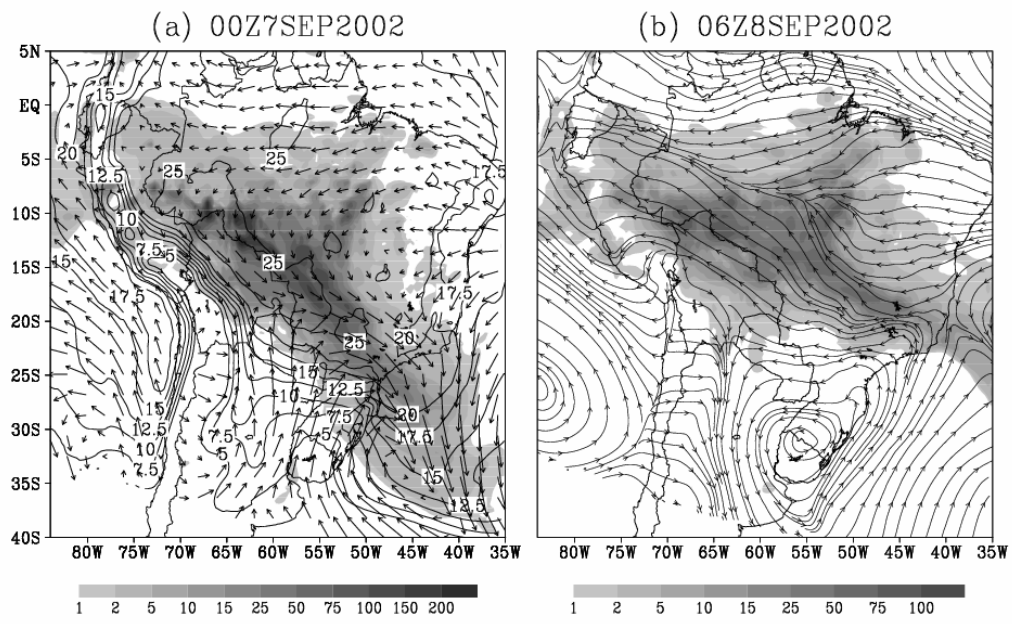


Figure 6

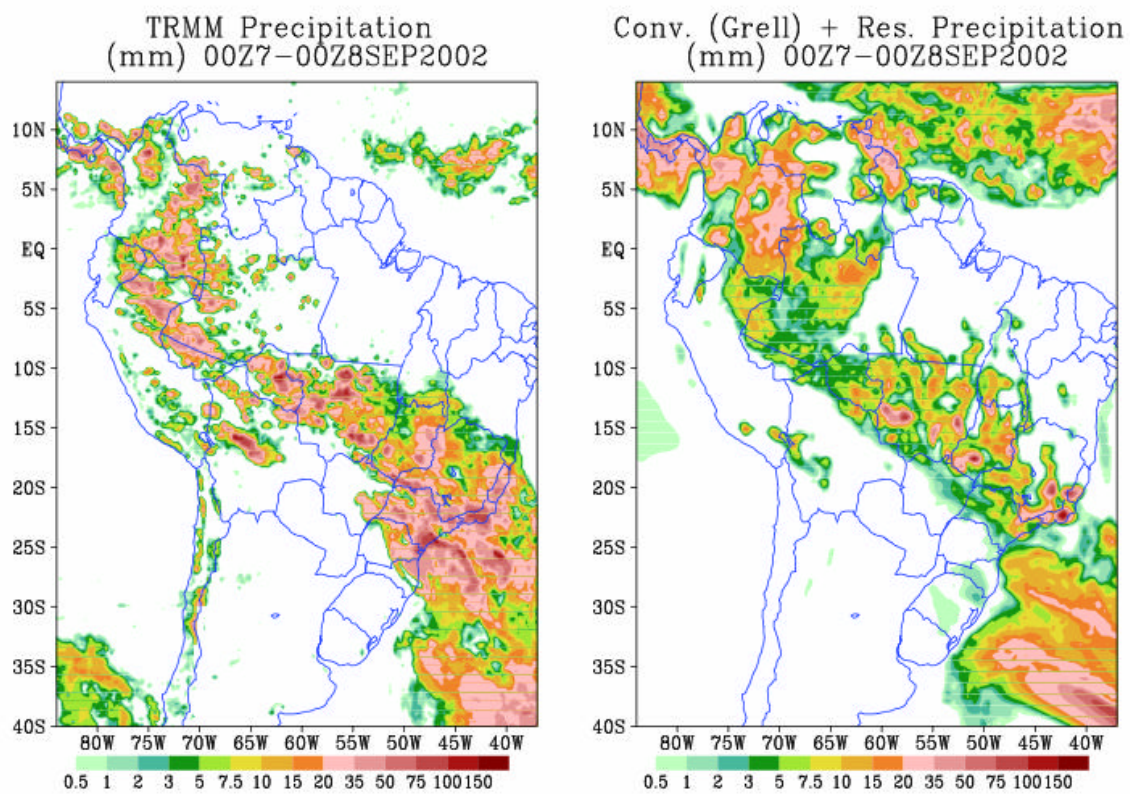


Figure 7

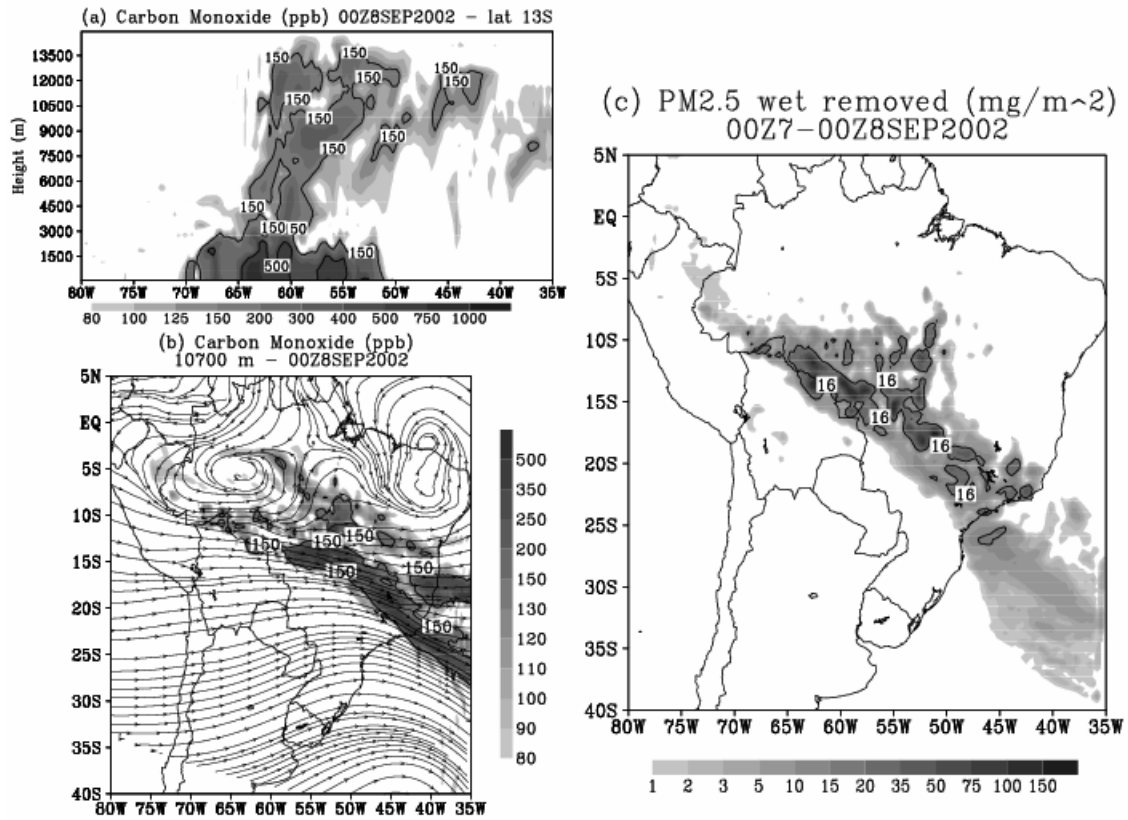


Figure 8

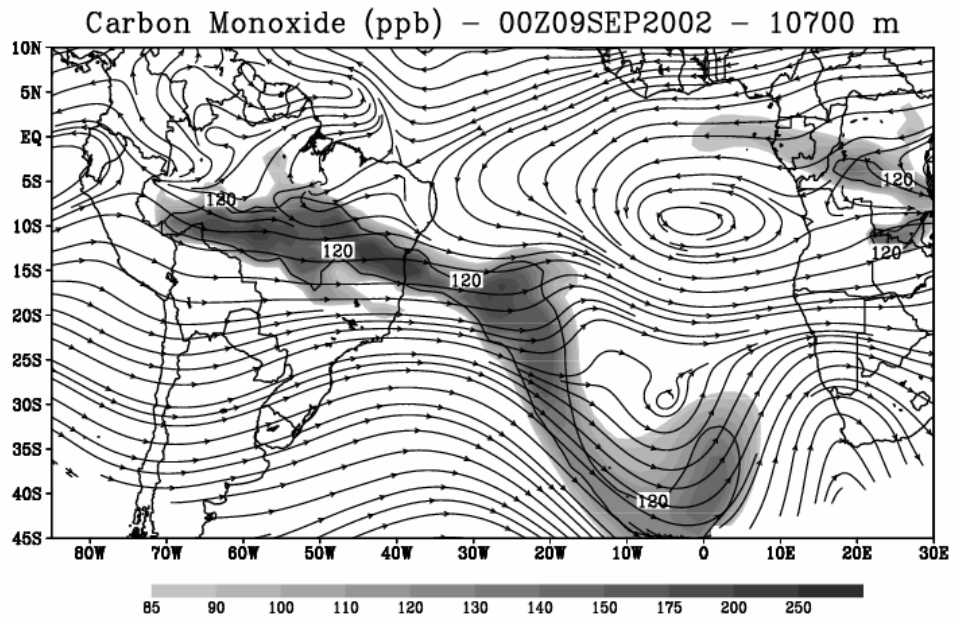


Figure 9

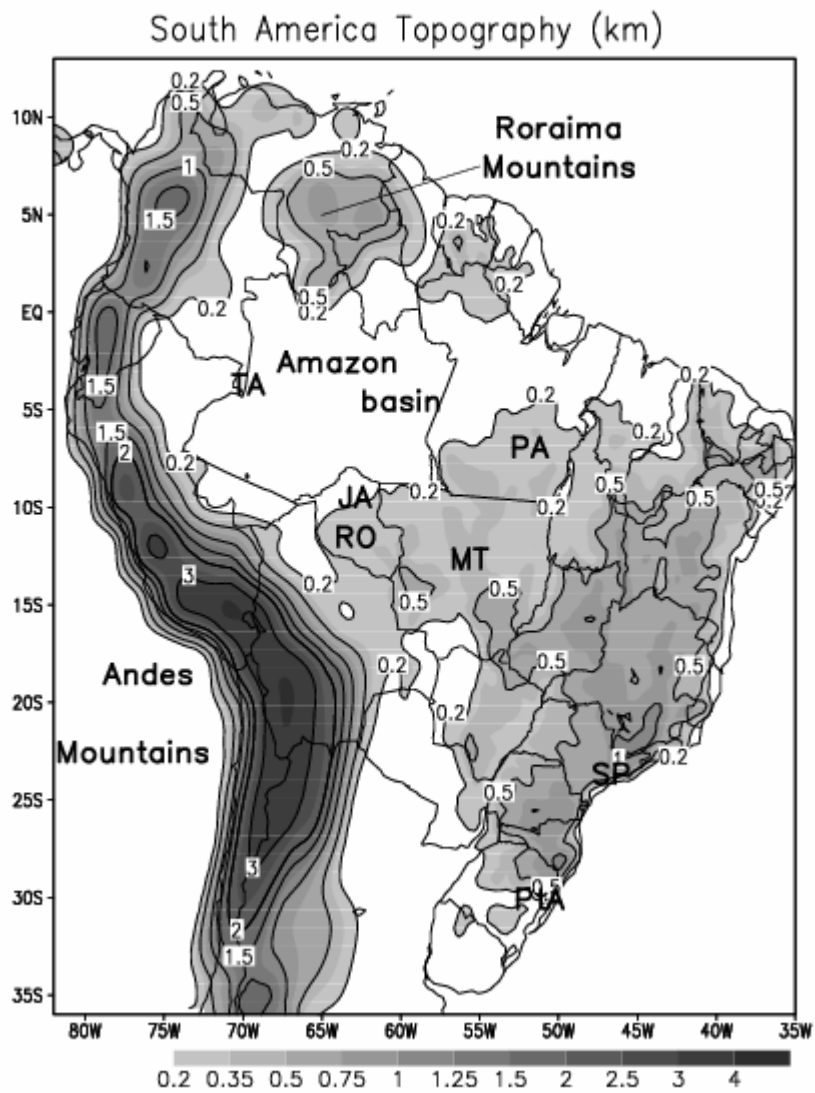


Figure 10

Carbon Monoxide Emission (ton/km²/month)

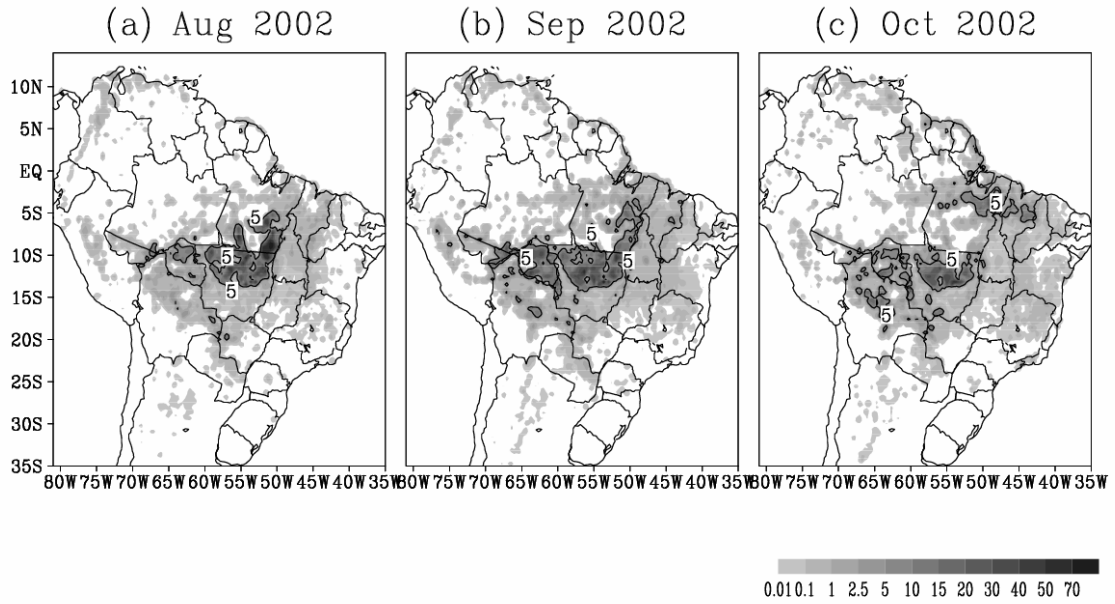


Figure 11

Mean Wind & Column PM2.5 (mg/m²)

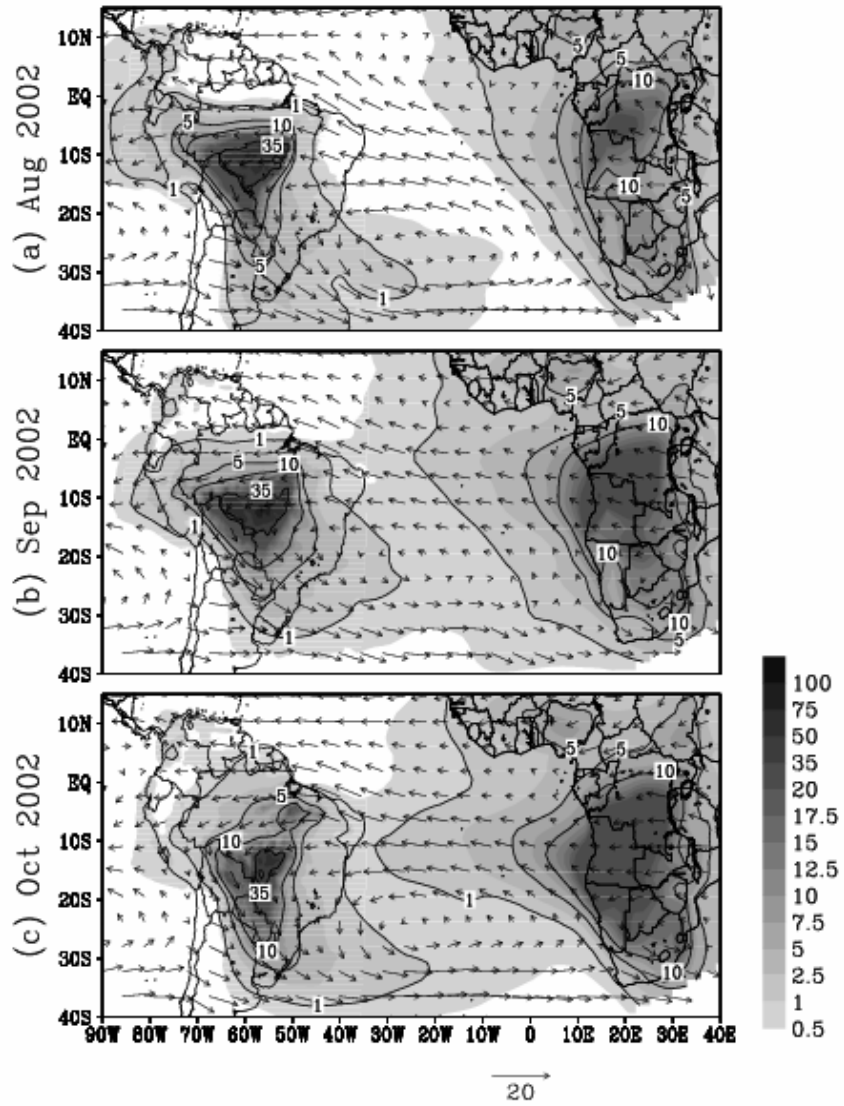


Figure 12

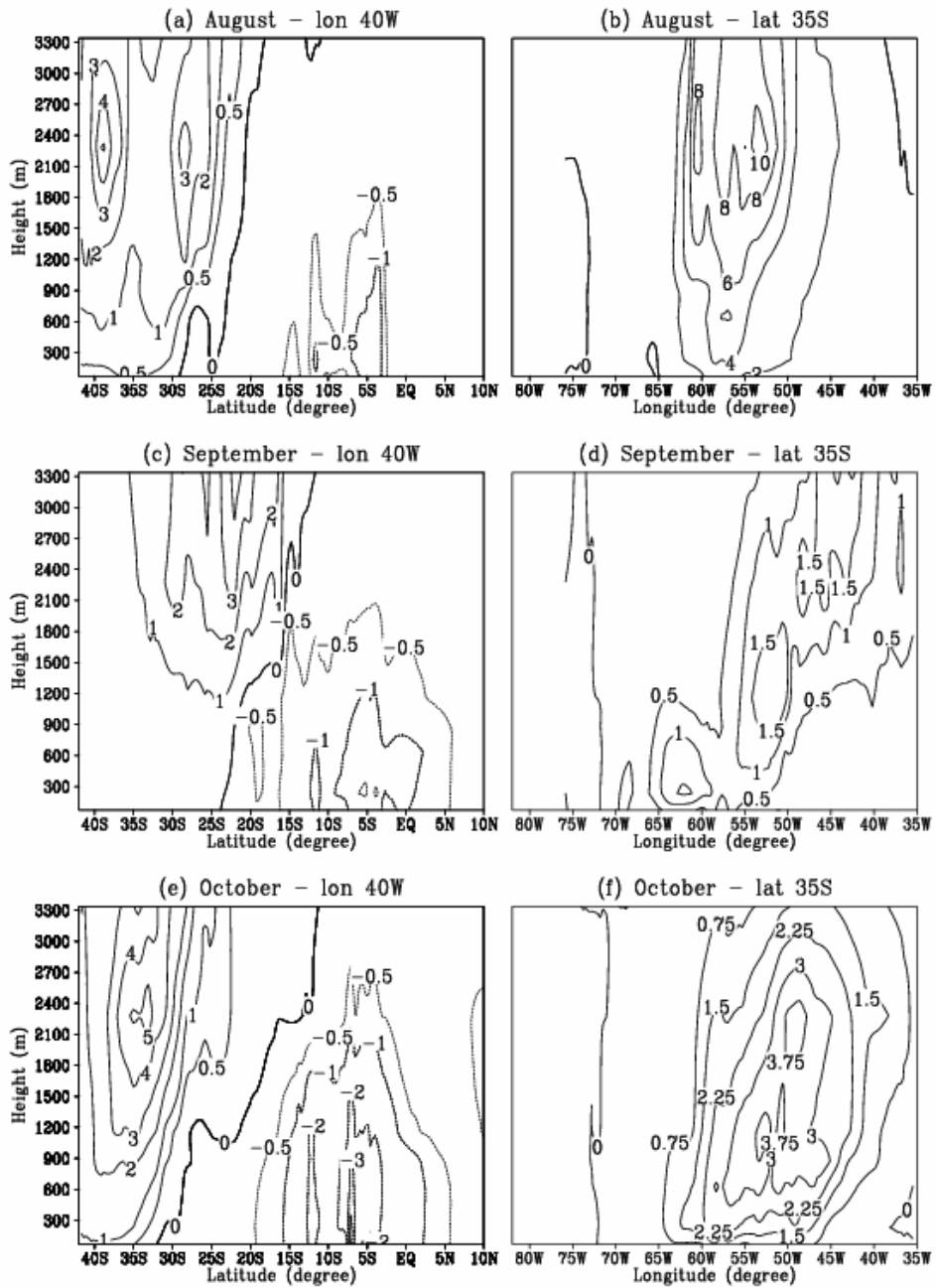


Figure 13

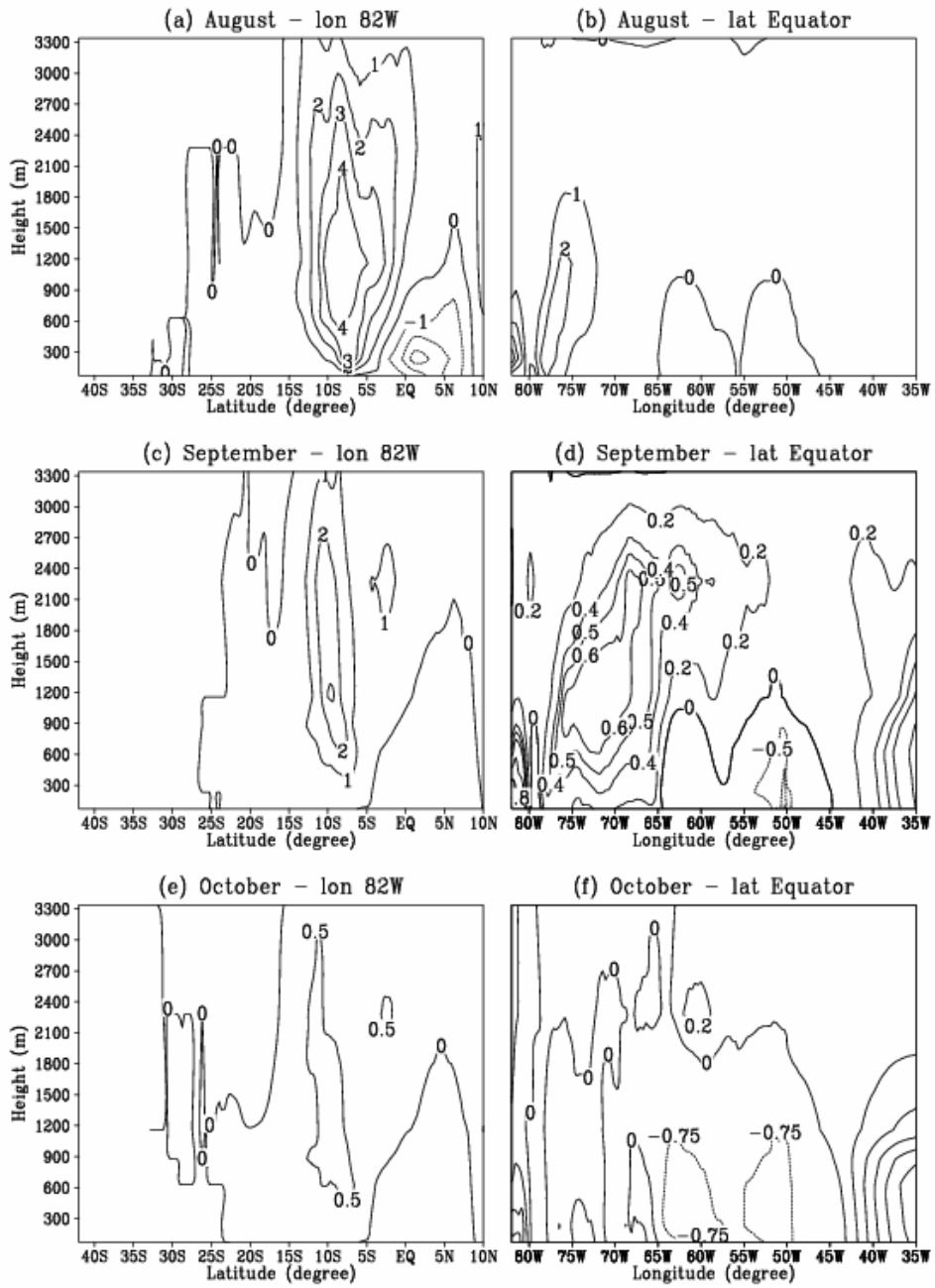


Figure 14

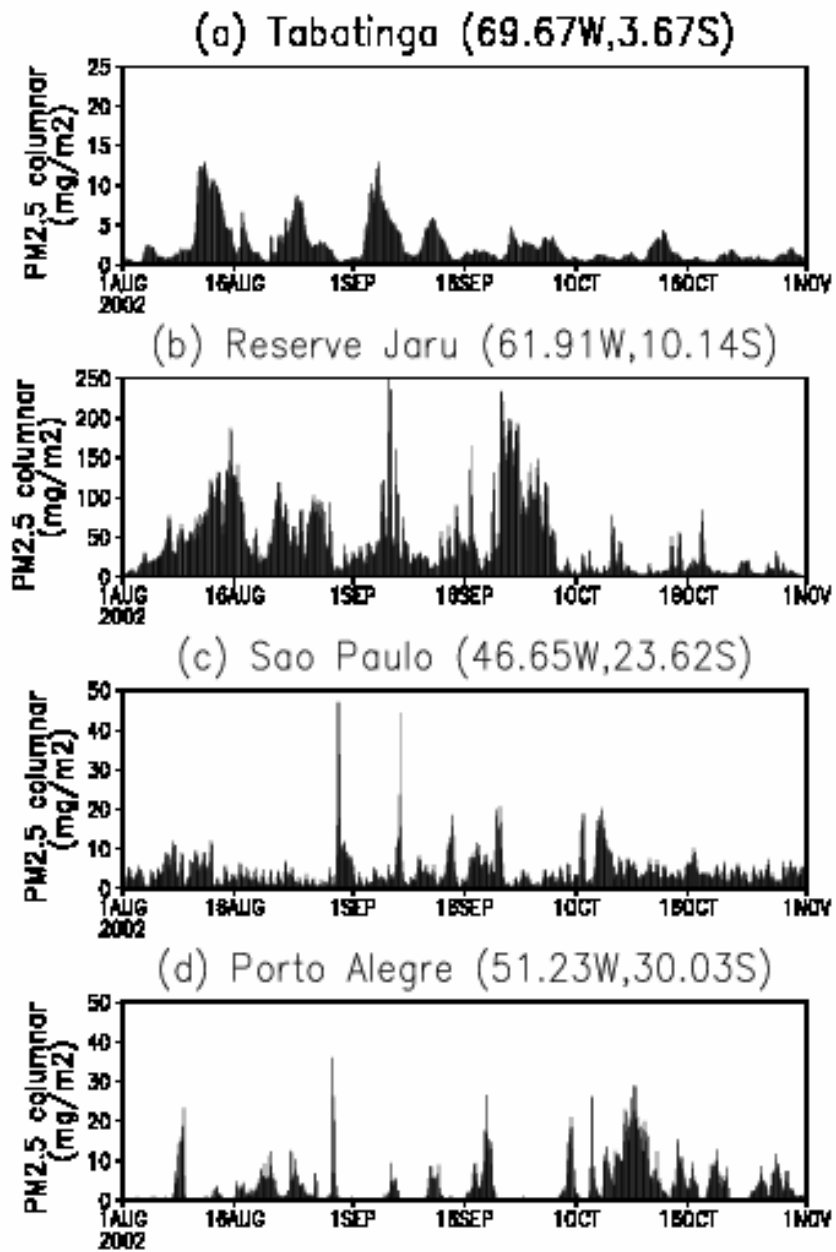


Figure 15

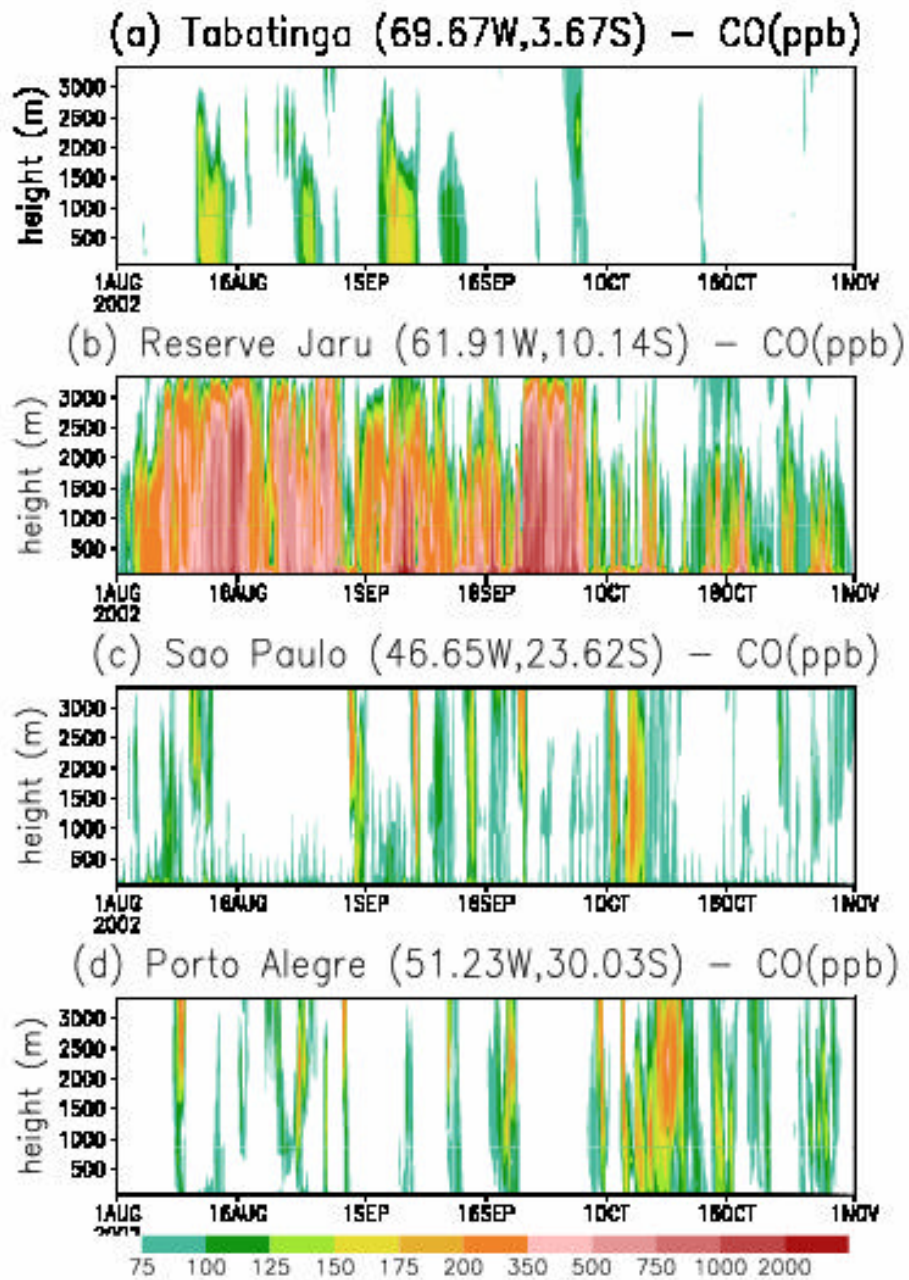


Figure 16

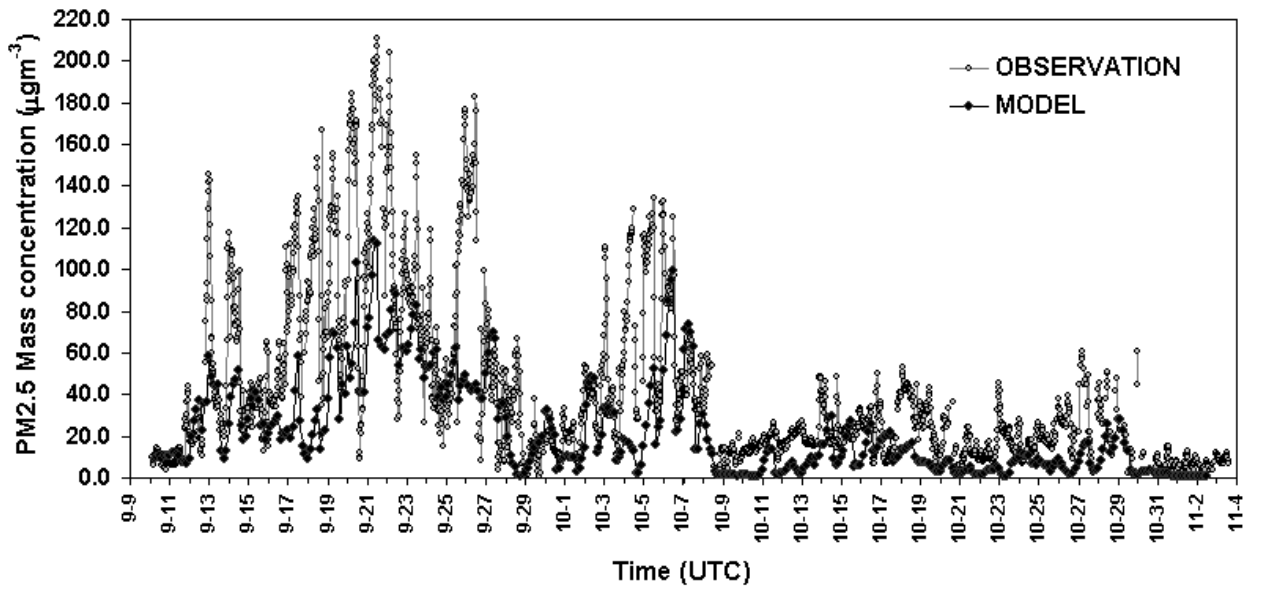


Figure 17